Supporting Information for "Alignment for Comprehensive Two-Dimensional Gas Chromatography with Dual Secondary Columns and Detectors (GCx2GC)" [Submitted to *Analytical Chemistry*.]

Stephen E. Reichenbach,[*] Davis W. Rempe,[*] Qingping Tao,[†] Davide Bressanello,[‡] Erica Liberto,[‡] Carlo Bicchi,[‡] Stefano Balducci,[§] Chiara Cordero[‡]

*University of Nebraska – Lincoln, Lincoln NE 68588-0115, USA

†GC Image, LLC, Lincoln NE 68505-7403, USA

‡Università degli Studi di Torino, I-10125 Torino, Italy

§La Sapienza University, Rome, Italy

ABSTRACT: This document provides supporting information for the paper "Alignment for Comprehensive Two-Dimensional Gas Chromatography with Dual Secondary Columns and Detectors (GCx2GC)", for the journal *Analytical Chemistry*. Due to space constraints and for brevity of presentation, the body of that paper presents results for only a few examples. This supplement provides additional results. This supplement also presents results for the maximum alignment error, which supplements the results for the average alignment error presented in the body of the paper. For a description of the samples, instrumentation, system settings, data preprocessing, alignment algorithms, and evaluation methodology, as well as references, refer to the body of the paper.

Review of Local Alignment Methods for GCxGC. Many local alignment methods have been proposed for GCxGC chromatographic data. One of the earliest methods used simple retention-time shifting to realize minimum pseudorank, with interpolation of the data for subpixel shifts (7). Dynamic Time Warping (DTW) (8) and Correlation Optimized Warping (COW) (9) were originally applied to one-dimensional signals then adapted for GCxGC (10,11). DTW uses dynamic programming to define a non-linear warping path to align two signals. For GCxGC, Vial et al. (10) applied DTW to the more variable second-column chromatograms. In developing COW, Nielsen (9) noted that the DTW distance measure relies on similar peak heights in the two chromatograms to give a reliable alignment (or on extensive pretreatment). COW segments one of the signals and uses correlation to assess piecewise linear warping of each segment to align with the other signal. Dynamic programming is used to solve the combinatorial optimization for all segments to have consistent start and end points without overlaps or gaps. Zhang et al. (11) applied COW separably in two dimensions, effecting piecewise bilinear interpolation. Both of these local methods require time-consuming computations. Wang et al. (12) developed a local alignment algorithm based on landmark peaks using distance and spectrum correlation optimization (DISCO). Although DISCO was developed for peak matching, it defines a retention-times mapping function in which the retention-times plane is segmented using the positions of landmark peaks, then piecewise linear interpolation is used to interpolate the retention-times of non-landmark peaks. Gros et al. (13) developed a landmark-based local alignment algorithm using Sibson natural-neighbor interpolation (14), based on a Voronoi diagram defined by landmark peaks. Recently, Furbo et al. (15) developed a local alignment method in which the correlation-optimized shift for each second-dimension chromatogram is computed and then those shifts are fit by a polynomial function. These local methods have varying levels of representational power, but all are more computationally expensive than simple global methods and cannot simply capture global structure.

Additional Results for Calibration Chromatograms. Figure S1 shows the results for alignment of an additional pair of consecutive replicate calibration runs (with concentration 100 mg/L). The alignment of chromatograms from the same detector in consecutive replicate runs provide benchmarks for subsequent alignment of the chromatograms from the flame ionization detector (FID) and mass spectrometer (MS) from a single GCx2GC-FID/MS run. For consecutive replicate calibration runs 2 and 3, the ^{1}D misalignment is about 0.041 min (or $0.7\times{}^1\sigma$); and, the ^{2}D misalignment is about 0.043 sec (or $0.5\times{}^2\sigma$) for the MS (which has a lower sampling frequency than the FID). These benchmarks are in line with those in the paper (although slightly higher for ^{1}D).

Figure S2 illustrates the performance for aligning FID and MS GCx2GC chromatograms from the same calibration run. As expected, for ^{1}D, none of the models yields any improvement in the testing set. As for the example in the paper, the ^{1}D misalignment is approximately equal to the stochastic modulation sampling noise level (0.024 min). For ^{2}D, all of the transformation models significantly improved alignment from about 0.14 sec (or $1.6\times{}^2\sigma$) before transformation to about 0.05 sec (or $0.6\times{}^2\sigma$) or less, with the second-degree polynomial approaching the benchmark of 0.043 sec. These results are consistent with those presented in the paper.

Tables S1 and S2 document the retention times and ^{1}D linear retention indices (LRIs) of calibration compounds in run #1 before and after alignment for all methods.

Additional Results for Urine Sample Chromatograms. Figure S3 shows the alignment results for another pair of consecutive replicate runs of one of the urine samples, which are used to establish benchmarks. For ^{1}D, the benchmark is about 0.026 min (or about $0.4\times{}^1\sigma$); and, for ^{2}D, the benchmark is about 0.038 sec (or about $0.4\times{}^2\sigma$) for the MS (which has a lower sampling frequency than the

FID). These results are in line with those in the paper (although slightly higher for ^{2}D).

Figure S4 shows the alignment performance for two GCx2GC runs of a urine sample. For ^{1}D, the misalignment of the FID and MS chromatograms is at the benchmark (about 0.03 min or $0.5\times{}^1\sigma$) without transformation and, as expected, none of the models reduces misalignment. For ^{2}D, the misalignment before transformation is large, about 0.25 sec or $2.9\times{}^2\sigma$, several times the benchmark. All of the transformation models significantly improve alignment. Affine transformation reduces misalignment by about two-thirds, to 0.09 sec (or $1.0\times{}^2\sigma$), but does not achieve the benchmark. Both polynomial transformations reduce misalignment to about 0.035 sec (or $0.4\times{}^2\sigma$), which is the benchmark for consecutive replicate sample runs. These results are consistent with those presented in the paper.

Maximum Alignment Error. Results for the root-mean-square error (RMSE) indicate average performance. The worst-case error also is of interest. Figures S5–S7 present the maximum absolute alignment error for any peak pair in any of the cross-validation runs for GCx2GC alignment, with Figure S5 for the calibration runs, Figure S6 for sample 41 runs, Figure S7 for sample 50 runs.

In all of these graphs, the size of the training set increases from left to right and the size of the testing set decreases from left to right, so there generally is an increase in the maximum error from left to right in the training set and a decrease in the maximum error in the testing set. Those trends are not of interest. Instead, the graphs should be viewed with an eye to the relative performance indicated by the four lines.

For ^{1}D, in all of the examples, if the training set is large enough, then the maximum absolute error for the testing set is about the same for all functions. For 2D, if the training set is large enough, then the maximum absolute error for the testing set is reduced by the affine transformation but is not as small as for the second-degree and third-degree polynomials, which perform similarly. As expected, the affine transformation requires the smallest training set and the third-degree polynomial requires the largest training set. These worst-case results are consistent with the results for mean performance. Also, the standard deviation of the maximum absolute error (computed over the iterations of leave-one-out cross-validation) was reduced by the affine transform but is not as small as for the second-degree and third-degree polynomials.

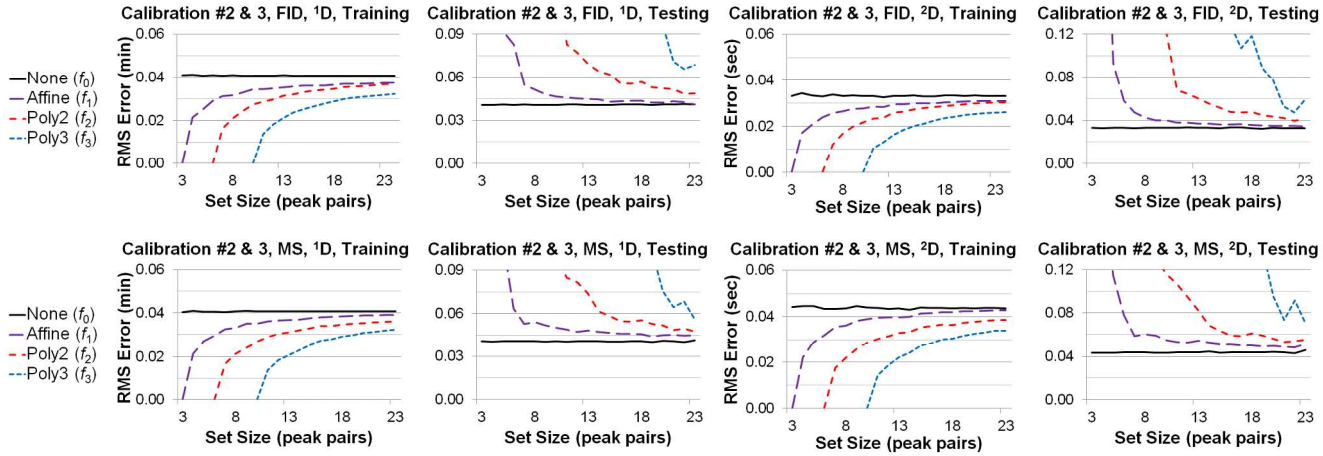

Figure S1: Cross-validation RMSE results as a function of the training set size for alignment of consecutive, replicate calibration chromatograms from the same detector. Columns from left to right are for ^{1}D with the training set, for ^{1}D with the testing set, for ^{2}D with the training set, and for ^{2}D with the testing set. The top row is for the FID chromatograms of calibration runs #2 and #3 and the bottom row is for the MS chromatograms of calibration runs #2 and #3.

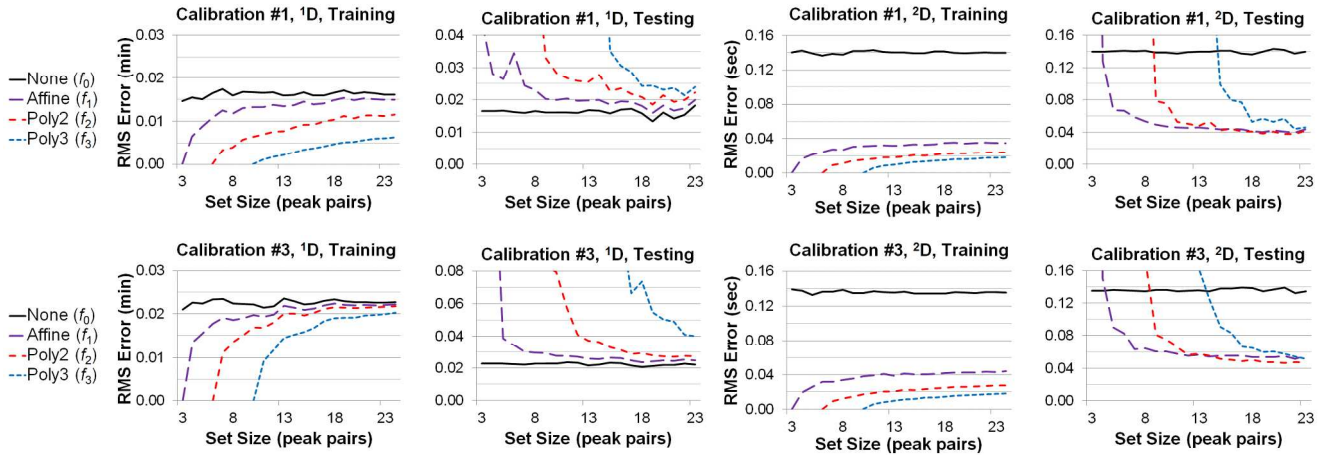

Figure S2: Cross-validation RMSE results as a function of the training set size for alignment of GCx2GC calibration chromatograms (from different detectors). Columns from left to right are for ^{1}D with the training set, for ^{1}D with the testing set, for ^{2}D with the training set, and for ^{2}D with the testing set. The top row is for the FID and MS chromatograms of calibration run #1 and the bottom row is for the FID and MS chromatograms of calibration run #3.

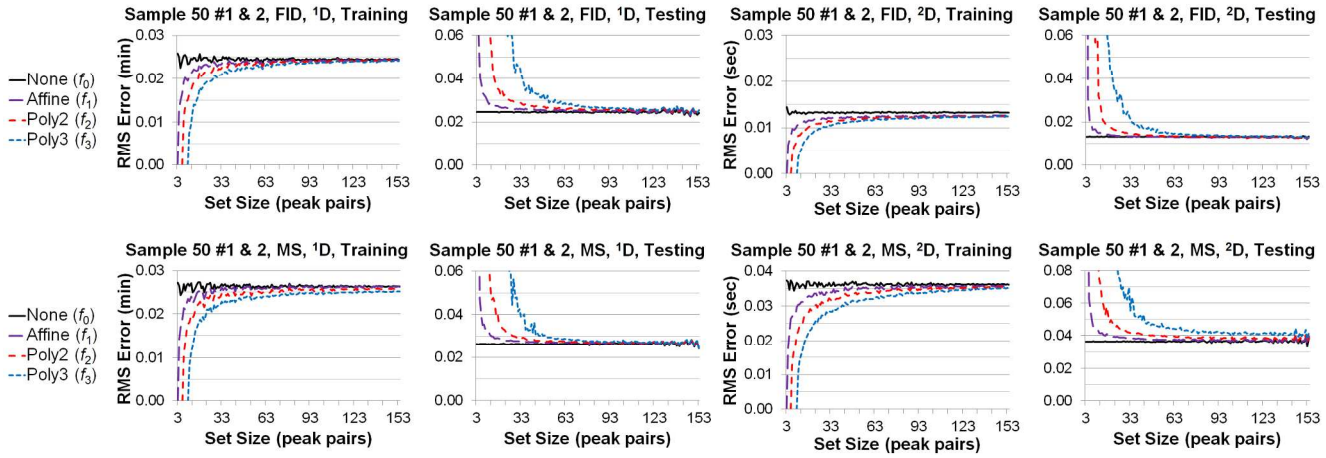

Figure S3: Cross-validation RMSE results as a function of the training set size for alignment of consecutive, replicate urine sample chromatograms from the same detector. Columns from left to right are for [1]D with the training set, for [1]D with the testing set, for [2]D with the training set, and for [2]D with the testing set. The top row is for the FID chromatograms of sample 50, runs #1 and #2, and the bottom row is for the MS chromatograms of sample 50, runs #1 and #2.

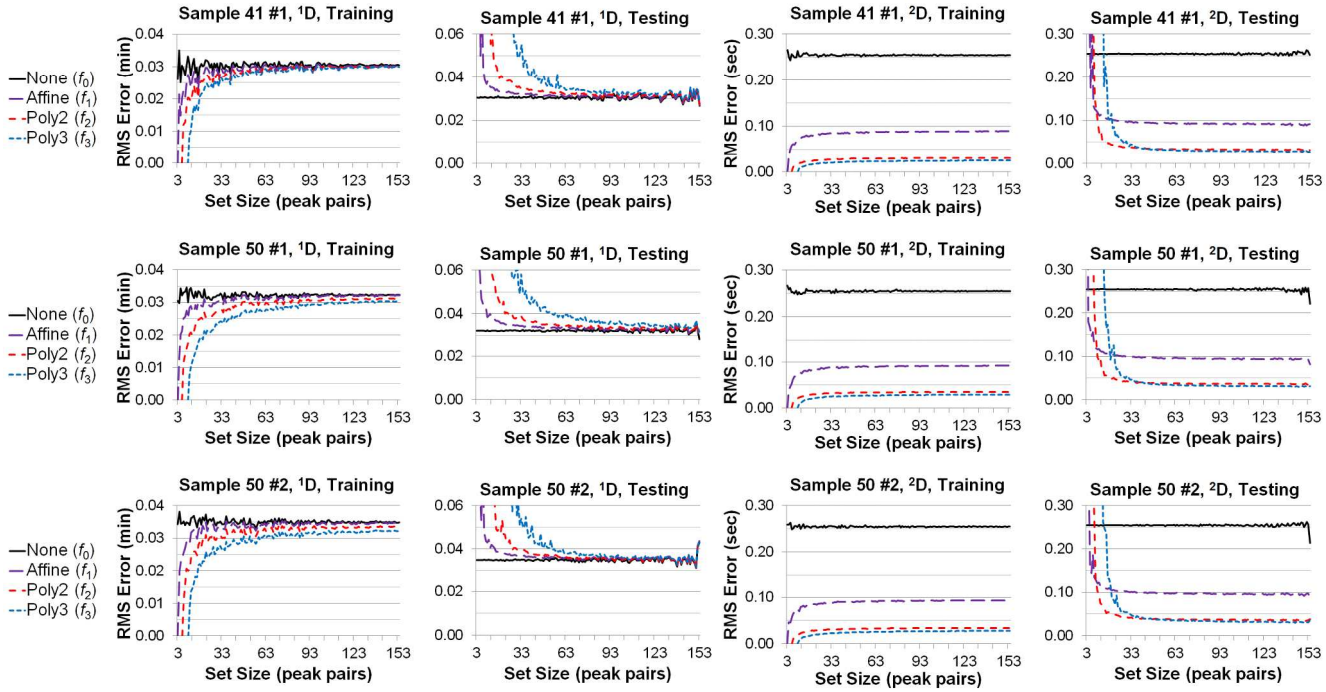

Figure S4: Cross-validation RMSE results as a function of the training set size for alignment of GCx2GC urine sample chromatograms (from different detectors). Columns from left to right are for [1]D with the training set, for [1]D with the testing set, for [2]D with the training set, and for [2]D with the testing set. Rows from top to bottom are for the FID and MS chromatograms of sample 41, run #1; for the FID and MS chromatograms of sample 50, run #1; and for the FID and MS chromatograms of sample 50, run #2.

A. Calibration #1.

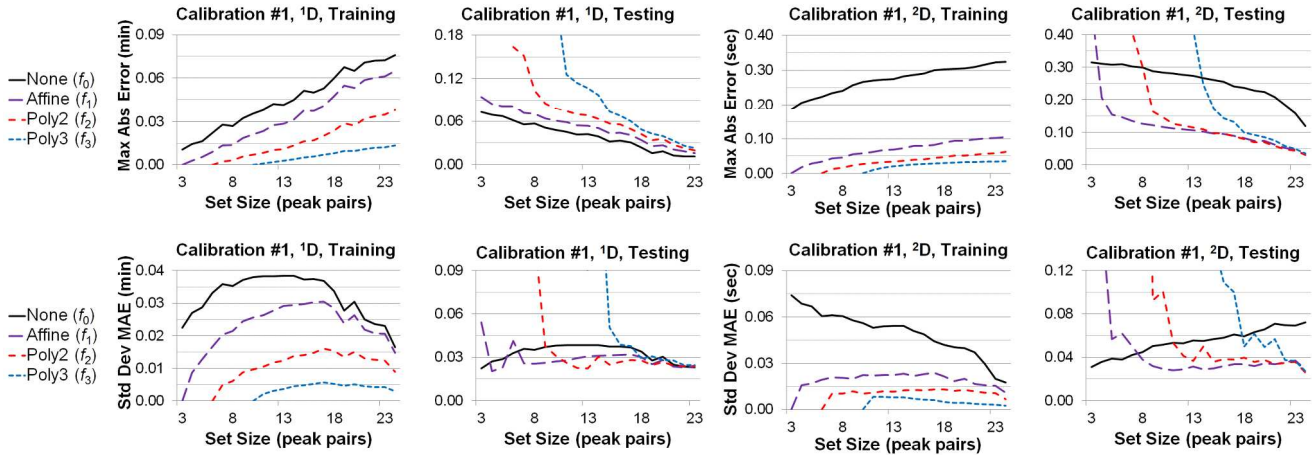

B. Calibration #2.

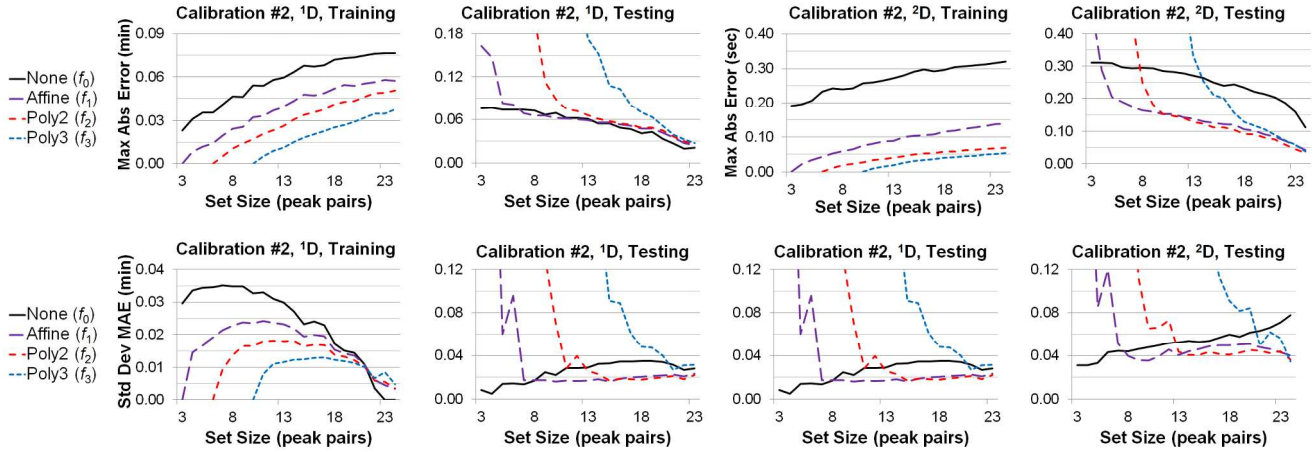

C. Calibration #3.

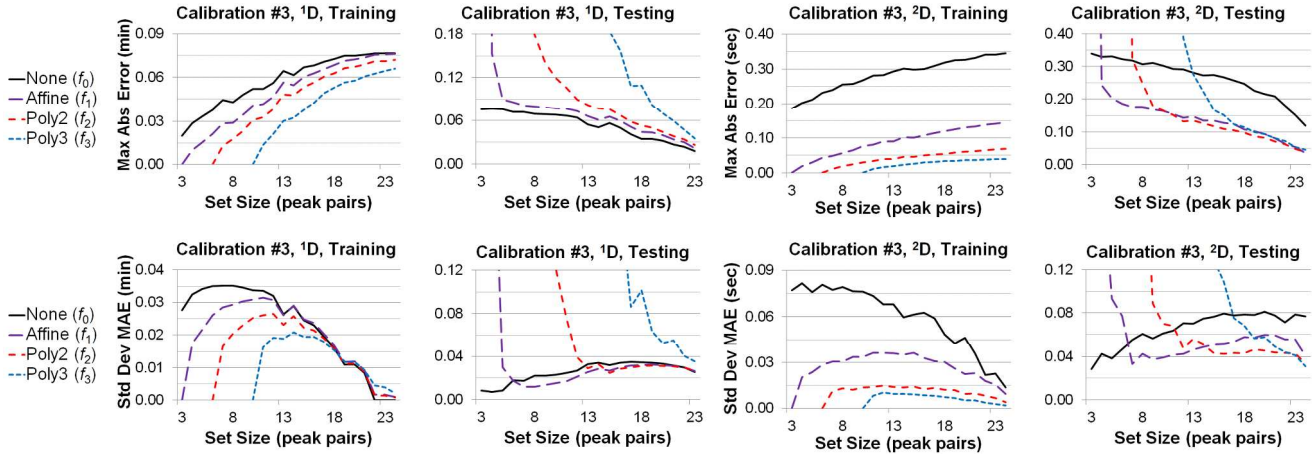

Figure S5: Maximum absolute error as a function of the training set size for alignment of GCx2GC calibration chromatograms (from different detectors). Columns from left to right are for ^{1}D with the training set, for ^{1}D with the testing set, for ^{2}D with the training set, and for ^{2}D with the testing set. Sets of rows with maximum absolute error on the top row of each set and the standard deviation of maximum absolute error on the bottom row of each set are for: A. Calibration #1, B. Calibration #2, and C. Calibration #3.

A. Sample 41, Run #1.

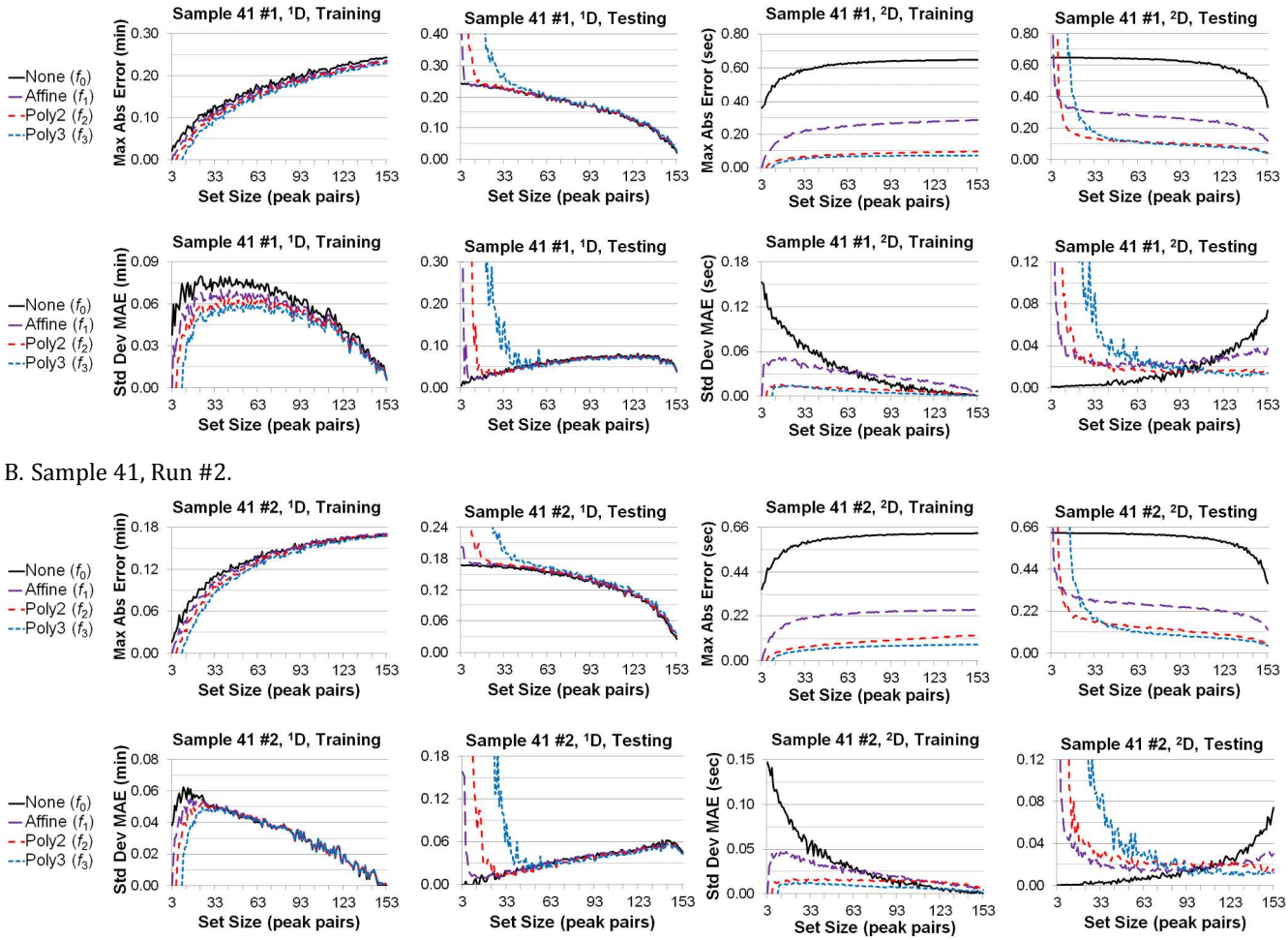

B. Sample 41, Run #2.

Figure S6: Maximum absolute error as a function of the training set size for alignment of GCx2GC urine sample #41 chromatograms (from different detectors). Columns from left to right are for ^{1}D with the training set, for ^{1}D with the testing set, for ^{2}D with the training set, and for ^{2}D with the testing set. Sets of rows with maximum absolute error on the top row of each set and the standard deviation of maximum absolute error on the bottom row of each set are for: A. Sample 41, Run #1, and B. Sample 41, Run #2.

C. Sample 50, Run #1.

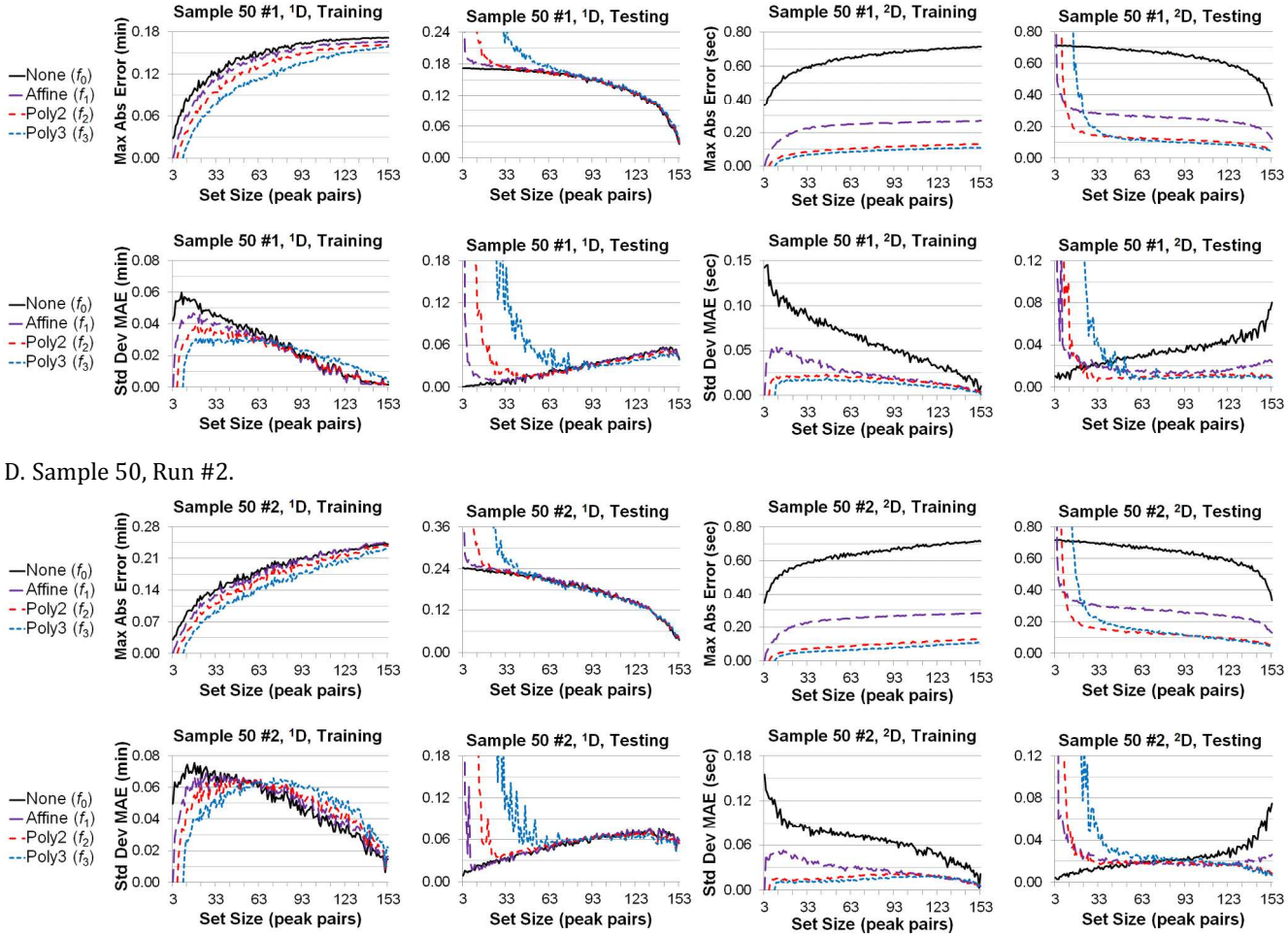

D. Sample 50, Run #2.

Figure S7: Maximum absolute error as a function of the training set size for alignment of GCx2GC urine sample #50 chromatograms (from different detectors). Columns from left to right are for ^{1}D with the training set, for ^{1}D with the testing set, for ^{2}D with the training set, and for ^{2}D with the testing set. Sets of rows with maximum absolute error on the top row of each set and the standard deviation of maximum absolute error on the bottom row of each set are for: A. Sample 50, Run #1, and B. Sample 50, Run #2.

Table S1 Transformations of the 25 target peaks in calibration #1 from the GCx2GC-MS chromatogram to align with corresponding peaks from the GCx2GC-FID chromatogram.

	FID (f_0)			***MS→FID Affine (f_1)***			***MS→FID Poly2 (f_2)***			***MS→FID Poly3 (f_3)***		
Compound Name	^{1}D Rt (min)	^{2}D Rt (sec)	^{1}D LRI	^{1}D Rt (min)	^{2}D Rt (sec)	^{1}D LRI	^{1}D Rt (min)	^{2}D Rt (sec)	^{1}D LRI	^{1}D Rt (min)	^{2}D Rt (sec)	^{1}D LRI
Pyruvic acid	8.92	3.50	1070	8.92	3.53	1070	8.91	3.54	1070	8.92	3.52	1070
Lactic acid	9.25	3.35	1081	9.25	3.35	1081	9.25	3.33	1081	9.25	3.33	1081
Alanine	10.58	3.32	1122	10.59	3.33	1122	10.58	3.31	1122	10.58	3.31	1122
Malonic acid	14.00	4.40	1224	14.00	4.33	1224	13.99	4.41	1223	14.01	4.41	1224
Valine	14.33	3.40	1233	14.34	3.38	1233	14.33	3.38	1233	14.33	3.38	1233
Leucine	16.33	3.40	1290	16.33	3.41	1290	16.33	3.42	1290	16.33	3.43	1290
Glycerol	16.67	2.89	1300	16.67	2.93	1300	16.68	2.89	1300	16.67	2.91	1300
Proline	16.92	3.49	1307	16.92	3.47	1307	16.92	3.49	1307	16.92	3.49	1307
Glycine	17.33	3.24	1320	17.33	3.26	1320	17.34	3.26	1320	17.33	3.26	1320
Succinic acid	17.67	4.25	1330	17.67	4.17	1330	17.67	4.22	1330	17.66	4.23	1330
Threonine	20.42	3.18	1413	20.42	3.18	1413	20.42	3.17	1413	20.41	3.18	1413
Malic acid	23.75	3.58	1515	23.75	3.54	1515	23.75	3.54	1515	23.76	3.54	1515
Creatinine	25.33	3.54	1564	25.33	3.55	1564	25.33	3.54	1564	25.34	3.54	1564
2-Ketoglutaric acid	26.33	3.73	1595	26.33	3.81	1595	26.34	3.79	1595	26.32	3.79	1594
Phenylalanine	27.50	3.64	1629	27.50	3.62	1629	27.50	3.60	1629	27.50	3.60	1629
Xylitol	30.75	2.31	1725	30.74	2.31	1725	30.75	2.29	1725	30.76	2.28	1725
Ribitol	31.25	2.27	1740	31.24	2.27	1740	31.25	2.26	1740	31.26	2.24	1740
ISTD (F-Phe)	32.50	3.44	1777	32.49	3.54	1777	32.50	3.49	1777	32.50	3.49	1777
Hippuric Acid	33.67	0.81	1813	*	*	*	*	*	*	*	*	*
Tyrosine I[a]	35.08	3.49	1859	35.08	3.50	1859	35.08	3.44	1859	35.08	3.44	1859
Fructose	35.83	1.90	1884	35.82	1.90	1883	35.83	1.91	1883	35.84	1.90	1884
Glucose	36.58	1.92	1909	36.57	1.92	1908	36.57	1.93	1908	36.58	1.93	1909
Mannitol	37.00	1.91	1924	36.99	1.91	1924	36.99	1.93	1924	36.99	1.93	1924
Tyrosine II[b]	37.00	2.55	1924	36.99	2.59	1924	36.97	2.59	1923	36.99	2.58	1924
Galactose	37.50	1.81	1942	37.49	1.80	1942	37.49	1.83	1942	37.49	1.83	1942
Myo Inositol	41.83	1.91	2110	41.90	1.80	2113	41.87	1.86	2112	41.84	1.89	2111

* Wraparound peak not included in transformation.

[a] Derivative I: trimethylsilyl ester of O-trimethylsilyl-tyrosine

[b] Derivative II: trimethylsilyl ester of N,O-bis(trimethylsilyl)-tyrosine

Table S2 Transformations of the 25target peaks in calibration #1 from the GCx2GC-FID chromatogram to align with corresponding peaks from the GCx2GC-MS chromatogram.

	MS Full-Scan (f_0)			FID→MS Affine (f_1)			FID→MS Poly2 (f_2)			FID→MS Poly3 (f_3)		
Compound Name	^{1}D Rt (min)	^{2}D Rt (sec)	^{1}D LRI	^{1}D Rt (min)	^{2}D Rt (sec)	^{1}D LRI	^{1}D Rt (min)	^{2}D Rt (sec)	^{1}D LRI	^{1}D Rt (min)	^{2}D Rt (sec)	^{1}D LRI
Pyruvic acid	8.92	3.70	1070	8.92	3.66	1070	8.93	3.65	1071	8.92	3.68	1070
Lactic acid	9.25	3.48	1081	9.25	3.48	1081	9.26	3.50	1081	9.26	3.51	1081
Alanine	10.59	3.48	1123	10.59	3.47	1122	10.59	3.49	1123	10.59	3.49	1123
Malonic acid	14.00	4.80	1224	14.00	4.89	1224	14.01	4.78	1224	14.00	4.80	1224
Valine	14.34	3.61	1233	14.34	3.64	1233	14.34	3.64	1233	14.34	3.63	1233
Leucine	16.34	3.70	1290	16.34	3.68	1290	16.34	3.68	1291	16.34	3.67	1291
Glycerol	16.67	3.10	1300	16.67	3.04	1300	16.65	3.11	1299	16.67	3.09	1300
Proline	16.92	3.78	1308	16.92	3.80	1307	16.92	3.79	1308	16.92	3.79	1307
Glycine	17.34	3.53	1320	17.34	3.50	1320	17.33	3.51	1320	17.34	3.49	1320
Succinic acid	17.67	4.67	1330	17.67	4.77	1330	17.67	4.71	1330	17.68	4.68	1330
Threonine	20.42	3.48	1413	20.42	3.48	1413	20.42	3.50	1413	20.42	3.48	1413
Malic acid	23.75	3.99	1515	23.76	4.05	1515	23.75	4.05	1515	23.75	4.06	1515
Creatinine	25.34	4.04	1564	25.34	4.03	1564	25.34	4.03	1564	25.33	4.05	1564
2-Ketoglutaric acid	26.34	4.38	1595	26.34	4.29	1595	26.33	4.30	1595	26.34	4.29	1595
Phenylalanine	27.50	4.16	1629	27.51	4.20	1629	27.50	4.22	1629	27.50	4.22	1629
Xylitol	30.75	2.59	1725	30.76	2.59	1725	30.75	2.61	1725	30.75	2.61	1725
Ribitol	31.25	2.55	1740	31.26	2.54	1740	31.25	2.57	1740	31.25	2.57	1740
ISTD (F-Phe)	32.50	4.16	1778	32.51	4.04	1778	32.51	4.08	1778	32.50	4.10	1777
Hippuric Acid	33.67	0.81	1813	*	*	*	*	*	*	*	*	*
Tyrosine I[a]	35.09	4.16	1859	35.09	4.15	1860	35.09	4.22	1860	35.09	4.20	1860
Fructose	35.84	2.17	1884	35.85	2.17	1884	35.84	2.16	1884	35.83	2.18	1884
Glucose	36.59	2.21	1909	36.60	2.21	1910	36.60	2.19	1909	36.59	2.20	1909
Mannitol	37.00	2.21	1924	37.02	2.20	1925	37.02	2.18	1925	37.02	2.18	1925
Tyrosine II[b]	37.00	3.06	1924	37.02	3.01	1925	37.03	3.01	1925	37.02	3.03	1925
Galactose	37.50	2.08	1942	37.52	2.09	1943	37.52	2.06	1943	37.51	2.07	1943
Myo Inositol	41.92	2.17	2114	41.85	2.30	2111	41.88	2.24	2112	41.91	2.19	2114

* Wraparound peak not included in transformation.

[a] Derivative I: trimethylsilyl ester of O-trimethylsilyl-tyrosine

[b] Derivative II: trimethylsilyl ester of N,O-bis(trimethylsilyl)-tyrosine